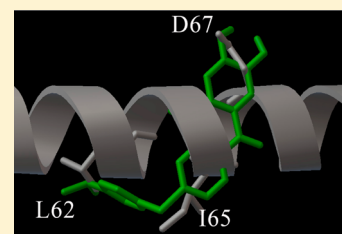


An Anthraquinone Scaffold for Putative, Two-Face Bim BH3 α -Helix MimicZhichao Zhang,^{*,†} Xiangqian Li,^{†,‡} Ting Song,[§] Yan Zhao,[§] and Yingang Feng^{||}[†]State Key Laboratory of Fine Chemicals, School of Chemistry, Dalian University of Technology, Dalian 116012, People's Republic of China[‡]State Key Laboratory of Natural and Biomimetic Drugs, Peking University, Beijing 100191, People's Republic of China[§]School of Life Science and Technology, Dalian University of Technology, Dalian 116024, People's Republic of China^{||}Qingdao Institute of BioEnergy and Bioprocess Technology, Chinese Academy of Sciences, Qingdao 266101, People's Republic of China;

Supporting Information

ABSTRACT: Bim BH3 peptide features an α -helix with hotspot residues on multiple faces. Compound **5** (6-bromo-2,3-dihydroxyanthracene-9,10-dione), which adopts a rigid-plan amphipathic conformation, was designed and evaluated as a scaffold to mimic two faces of Bim α -helix. It reproduced the functionalities of both D67 and I65 on two opposing helical sides. Moreover, it maintained the two-faced binding mode during further evolution. A putative BH3 α -helix mimic and nanomolar Bcl-2/Mcl-1 dual inhibitor, **6**, was obtained based on the structure of **5**.



INTRODUCTION

Protein–protein interaction (PPI) interfaces are attractive targets for therapeutic agents.^{1,2} Most multiprotein complexes feature α -helical segments at their interfaces.^{3,4} The hotspot residues, which contribute significantly to the binding energy between proteins, can be spatially distributed on one, two, or all three faces of an α -helix.³

The PPIs between anti- and pro-apoptotic Bcl-2 members are mediated by the α -helix of the BH3-only proteins.² The six known Bcl-2-like anti-apoptotic proteins are divided into two classes, represented by Bcl-2 and Mcl-1.^{5,6} They can bind to pro-apoptotic BH3-only proteins through the shared BH3 domain.^{7,8} Bim is a nonselective BH3-only protein that can neutralize both arms of the anti-apoptotic Bcl-2 family, Bcl-2 and Mcl-1 proteins.⁹ Therefore, small molecules that reproduce the spatial distribution of hotspots in the Bim BH3 peptide have been investigated for decades as potential antitumor drugs.^{10,11}

This is a challenge because the Bim BH3 peptide is an α -helix with hotspots on three faces, while small-molecule BH3 mimetics, including clinical candidates, fail to mimic multiple Bim faces. Crystallographic results have shown that ABT-737 can mimic hotspot residues only on one face of Bim (L62 and F69) to interact with the p2 and p4 pockets of the Bcl-X_L protein and cannot mimic D67 that is conserved in all BH3 domains. Additionally, it cannot hit Mcl-1.^{9,12} The reported binding modes of (–)-Gossypol are inconsistent, as is Apogossypol.^{13–15} No convincing two-face-mimicking features were shown by NMR-derived structures. Nonpeptide α -helix mimicry, including terphenyl scaffolds and their related structures, typically impart functionality from only one face of the helix.^{3,16,17}

To mimic multiple faces of the Bim BH3 α -helix with small molecules to inhibit both the Bcl-2 and Mcl-1 proteins in tumor cells, an anthraquinone platform compound **5** was obtained with a conserved two-face binding mode, on which a functional and structural Bim mimetic compound **6** was derived. Compound **6** exhibited nanomolar affinities toward the two proteins and specific antitumor ability in cells.

RESULTS AND DISCUSSION

Rationale. We sought to understand the hotspot distribution of Bim in complex with Mcl-1 and Bcl-2. Because the crystal structure of the Bim/Bcl-2 complex has not been reported, we used the isogenous protein Bcl-X_L, which has a similar three-dimensional architecture, in its place.^{18,19} We found that residues E55, I58, L62, R63, I65, D67, F69, and F73 are hotspots of Bim binding to both Mcl-1 and Bcl-X_L. These residues are located on two faces of the helix (Figure 1a,b; Figure S1 in Supporting Information). Among them, D67, I65, and L62 show the highest free energy penalty ($\Delta\Delta G_{\text{bind}} = 2.0\text{--}3.0 \text{ kcal}\cdot\text{mol}^{-1}$). W57 and E61 for Mcl-1 and Bcl-X_L, respectively, reside on the third face of the helix and are much less important for binding ($\Delta\Delta G_{\text{bind}} = 1.0 \text{ kcal}\cdot\text{mol}^{-1}$).³ We concluded that the mimicking of residues covered by D67 to I65 is important for a Bim mimetic.

In the hMcl-1/hBim complex, D67 can form a hydrogen bond with R263 of Mcl-1, while L62 and I65 occupy the hydrophobic p2 and p3 pockets, respectively.^{5,9} The p3 pocket located on the opposite side of R263 (or R146 in Bcl-2) and on

Received: October 17, 2012

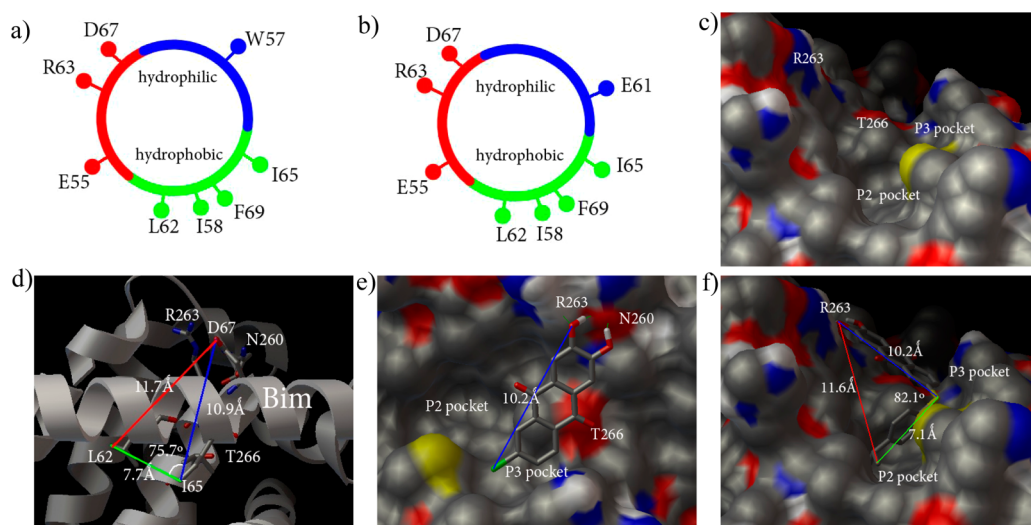


Figure 1. (a, b) Diagrams of hotspots in (a) Bim/Mcl-1 and (b) Bim/Bcl-XL. (c) Surface representation of the BH3 binding domain of Mcl-1 (side view). (d) Positions of hotspot residues in a ribbon diagram of the Bim/Mcl-1 complex (front view). (e, f) Docking results of Mcl-1 with (e) compound 5 (front view) and (f) compound 6 (side view). Carbon, oxygen, nitrogen, bromine, and sulfur atoms are colored gray, red, blue, green, and yellow, respectively. Hydrogen bonds are depicted as green dotted lines.

the edge of the groove. The p2 pocket is located in the bottom of the groove, and it is larger and deeper than p3 (Figure 1c,d).²⁰ Notably, D67 is the “hottest” residue of the Mcl-1 protein, and its mutation to alanine affects its binding affinity much more significantly than other hotspots.⁵ Additionally, our previous study indicated that mimicking D67 can contribute to Bcl-2/Mcl-1 dual inhibition by a small molecule.²¹

However, terphenyl-like scaffolds can only mimic the surface functionality projected along the bottom hydrophobic face, including L62, I58, and I65. All of these scaffolds lost the hydrophilic hotspot D67 on the opposite side of the α -helix.^{16,17} A main reason is that the width of these scaffolds (2.4 Å) is less than the diameter of the α -helix (4.6 Å), and the rigidity of these scaffolds might be not sufficient to allow the substituents to reach the most solvent-exposed residue, D67. The lack of this very hot residue may result in suboptimal affinity for the target. In addition, the free rotation between the phenyl rings of the terphenyl scaffolds always results in multiple conformations. As such, adaptive changes in conformation are required for these molecules to bind to the BH3 groove, which lead to a decrease in conformational entropy that is unfavorable for binding energy.^{22,23} Correspondingly, these “one-face” α -helix mimetics always exhibit weaker affinity in the micromolar range.^{2,24} A suitable scaffold for amphiphilic α -helix mimetics should facilitate the installation of functional groups on both sides of the scaffold and also ensure rigid conformation by its preorganized framework.²⁵

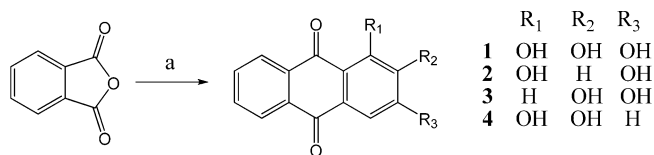
Structure-Based Design, Synthesis, and Evaluation.

We then constructed a molecular platform that is different from the terphenyl scaffolds and mimics the sagittal axis of the helix. We tried to mimic the helix such that it reproduces the arrangement of D67 and the opposite residue I65, which cover approximately 200° of the circle. We developed a rigid naphthalene ring, whose width (4.8 Å) is similar to the diameter of natural α -helix peptides. We hope this platform can serve as a bridge that spans from D67 to I65. We noticed that there is a small residue, G66, between D67 and I65 in the structure of the Bim BH3 peptide, corresponding to the hydrophilic, solvent-exposed residue T266 in Mcl-1 (Figure 1c,d).⁶ As such, a rigid, planar anthraquinone that is both

hydrophobic and hydrophilic is favorable. D67, at one end of the bridge, was considered first because a specific atom was needed to mimic a hydrophilic residue and to form a hydrogen bond. Another conserved residue, N260 in Mcl-1, a neighbor of R263 in the three-dimensional structure, was also conserved in the Bcl-2 protein (Figure 1d) and was selected to form an additional hydrogen bond to further stabilize the bridge.²⁶ Therefore, three adjacent hydroxyl groups were attached to anthraquinone to mimic the interactions of D67 with both Bcl-2 and Mcl-1. As the p3 pocket corresponding to I65 is on the other end of the bridge, a hydrophobic phenyl group was employed to occupy the p3 pocket.

On the basis above, compound 1 was synthesized by Friedel–Craft acylation, by reacting phthalic anhydride with pyrogallol in a molten homogeneous mixture of aluminum chloride and sodium chloride (Scheme 1).²⁷ We measured its

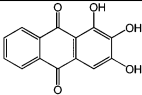
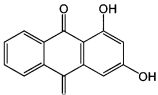
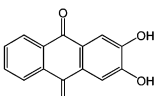
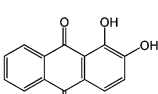
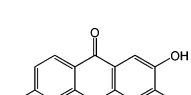
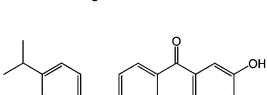
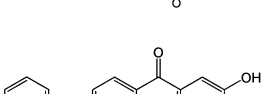
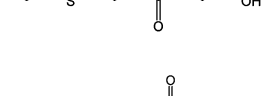
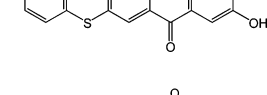
Scheme 1. Synthesis of Compounds 1–4^a



^aReagents and conditions: (a) AlCl₃, NaCl, substituted phenols, 160 °C, 4 h; 10% HCl, 100 °C.

binding to Mcl-1 and Bcl-2 by fluorescence polarization assays (FPAs) and found a K_i of 270 nM for Mcl-1 and 583 nM for Bcl-2 (Table 1; Figure S2 in Supporting Information). To identify which hydroxyls of pyrogallol are responsible for this function, compounds 2–4 were designed and synthesized by similar methods (Scheme 1). Except for compound 3, which maintained similar affinities to Mcl-1 and Bcl-2 as 1, the absence of either the 2- or 3- hydroxyl made compounds 2 and 4 lose most of their affinities (Table 1; Figure S2 in Supporting Information). This finding highlighted the necessity of these two neighboring hydroxyl groups, which can mimic a hydrogen-

Table 1. Structure and Binding Affinities of Small-Molecule Inhibitors to Mcl-1 and Bcl-2^a

Compounds	Structure	$K_i \pm SD$ (μM , Mcl-1)	$K_i \pm SD$ (μM , Bcl-2)
1		0.270±0.04	0.583±0.16
2		2.27±0.86	1.70±0.64
3		0.312±0.13	0.420±0.16
4		1.62±0.73	1.15±0.49
5		0.107±0.018	0.132±0.039
6		0.013±0.004	0.024±0.013
7		0.053±0.011	0.071±0.008
8		0.038±0.013	0.044±0.009
9		0.056±0.012	0.087±0.021

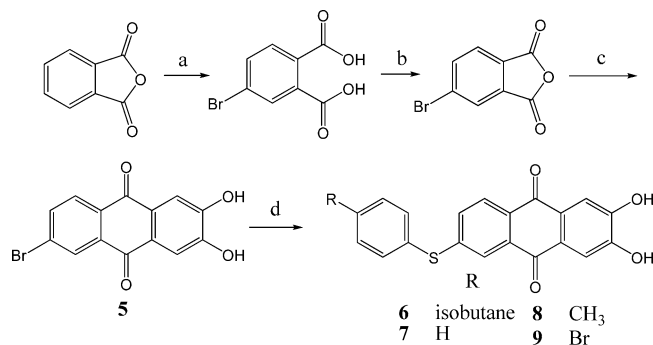
^aAs determined by fluorescence polarization assays.

bonding network formed by D67 and R263/N260 as predicted by the docking study (Figure S3 in Supporting Information).

From the predicted binding mode, the length of **3** is 8.6 Å, which is shorter than the maximum distance between D67 and I65 (10.9 Å in Mcl-1/Bim, Figure 1d and Figure S3b in Supporting Information; 10.4 Å in Bcl-X_l/Bim, not shown). We then extended **3** by attaching a bromine atom at the 6-position to probe the proper length of the p3 pocket. Compound **5** was synthesized by Friedel–Craft acylation following bromination (Scheme 2). The K_i value of **5** toward Mcl-1 (107 nM) is approximately 3-fold higher than that of **3** (312 nM) (Table 1; Figure S2a in Supporting Information). A similar improvement was found for Bcl-2 (Table 1; Figure S2b in Supporting Information). The docking study also suggested

that compound **5** has the proper length (10.2 Å) to span from R263 to the p3 pocket (Figure 1e).

Next, we performed heteronuclear single quantum coherence (HSQC) NMR spectroscopy, using ¹⁵N labeled Mcl-1 protein to identify the binding site of **5**. Two-dimensional (2D) ¹H–¹⁵N HSQC NMR spectra of Mcl-1 were recorded without (black) and with (green) compound **5** (Figure S4, Supporting Information). Figure 2a shows a plot of the chemical shift perturbations against the overall Mcl-1 protein residues. Approximately 70% of the residues that were perturbed above the threshold value (0.05 ppm) were located in the cleft of the Mcl-1 protein into which the Bim helix binds (Figure 2b). The residues of R263 and N260 and the neighboring residues V258 and V253 showed significant chemical shift ($\Delta\text{CS} > 0.05$ ppm)

Scheme 2. Synthesis of Compounds 5–9^a

^aReagents and conditions: (a) NaOH, H₂O, Br₂, 90 °C, 6 h; HCl. (b) Ac₂O, 140 °C, 2 h. (c) AlCl₃, NaCl, pyrocatechol, 160 °C, 4 h; 10% HCl, 100 °C. (d) 4-R-PhSH, K₂CO₃, CuI, DMF, 130 °C, 8 h, 10% HCl.

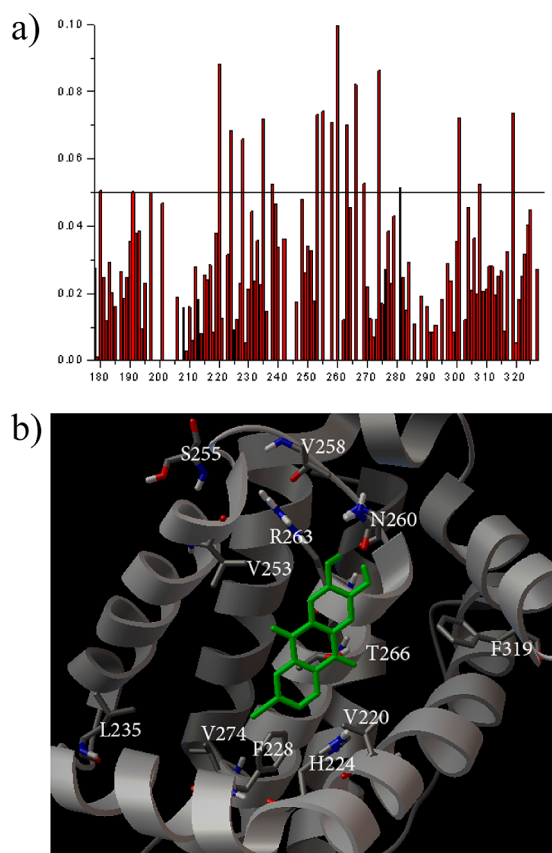


Figure 2. (a) Chemical shift perturbations of Mcl-1 residues bound to compound 5. (b) NMR-derived structure of 5 bound to Mcl-1. Mcl-1 residues with chemical shift changes $\Delta\text{CS} > 0.05$ ppm are shown, including R263, N260, and their nearby residues. V220, H224, F228, and T266 from the p3 pocket are also included.

changes upon the addition of compound 5. V220, H224, V274, and F228, which are located in the p3 pocket, also exhibited significant chemical shift perturbations. T266, in the middle of R263 and p3, was also significantly affected by 5. The NMR results demonstrated that 5 can mimic two hotspots in Bim, D67 and I65, which are located on the two faces of α -helix (Figure S5a, Supporting Information).

Together with the docking studies, the modest binding affinity, exact binding mode, and rigid structure provided

evidence that 5 can find its binding position and serve as a platform from which more substituents can project to mimic additional residues on other face of the Bim BH3 α -helix. L62, which is located in the deepest p2 pocket of the BH3 groove, was the next target. Cumene, benzene, toluene, and bromobenzene were introduced at the 6-position of compound 5. A rotatable sp³ hybrid sulfur atom, which is one of the most hydrophobic atoms, was employed as a linker to allow substituents to turn to the left (C terminal of Bim BH3 peptide) and penetrate into the bottom of BH3 groove (Figure 1f).

Compounds 6, 7, 8, and 9 were synthesized and evaluated in our FP-based binding assay (Scheme 2, Table 1). Excitingly, improved affinities were found for these analogues, and the greatest improvement was found for 6, which exhibited an 8-fold enhancement in K_i toward Mcl-1 (13 nM) and a net 6-fold improvement to Bcl-2 (24 nM) over 5 (Table 1; Figure S2 in Supporting Information). These improvements can be attributed to the similarity in shape and hydrophobicity of cumene with L62. A docking study found that compound 6 maintained the mimicry of D67 and I65 and achieved functional mimicry of an additional residue, L62, to occupy the p2 pocket in Mcl-1. Compound 6 reproduced a similar arrangement with L62, I65, and D67 in the Bim peptide (Figure 1d,f; Figure S5b in Supporting Information).

To confirm that 6 maintains the binding mode of 5, we performed 2D ¹H–¹⁵N HSQC NMR recorded without (black) and with (red) compound 6 (Figure S4, Supporting Information). With the addition of 6, approximately 80% of the residues that showed chemical shift changes $\Delta\text{CS} > 0.05$ ppm were located in the BH3 binding domain of the Mcl-1 protein (Figure 3). In addition to the chemical shifts of R263, N260, V258, T266, V220, and F228, which are the same for compound 5, residues M250 and F270, located in the bottom of the p2 pocket and corresponding to L62, are newly emergent residues with significant chemical shift perturbations ($\Delta\text{CS} > 0.05$ ppm). NMR identified the conserved binding mode of 5 and provided both a two-face Bim mimetic and a scaffold on which numerous derivatives mimicking multiple faces of Bim can be designed (Figure S5, Supporting Information).

The disruption of both Bcl-2/Bax and Mcl-1/Bak in ABT737-resistant Nalm-6 cells was verified by coimmunoprecipitation, and the results mirrored its *in vitro* pan-inhibition (Figure 4a). Because compound 6 occupies the BH3 groove, its pure BH3 mimicking property was identified through a cell-based shRNA assay, which showed that 6 completely killed the cells through Bax/Bak (Figure 4b). Consistent with its mechanism-based killing, a micromolar lethal effect was found in multiple cancer cell lines, while no significant cytotoxicity was found in the normal HEK293 cell line (Table S1, Supporting Information). Notably, 6 did not show DNA damage *in vitro* (Figure S6, Supporting Information) and induced apoptosis but not necrosis in cells (Figure S7, Supporting Information). These results illustrated that 6 is a functional and structural Bim mimetic.

The promising compound ABT-737 binds with high affinity ($K_i < 1$ nM) to Bcl-X_L and Bcl-2. Its IC₅₀ values range from submicromolar to micromolar depending on cell species.^{9,12,28} Compound 6 exhibited 3–7 μM IC₅₀ values on certain tumor cells in the present study (Table S1, Supporting Information).

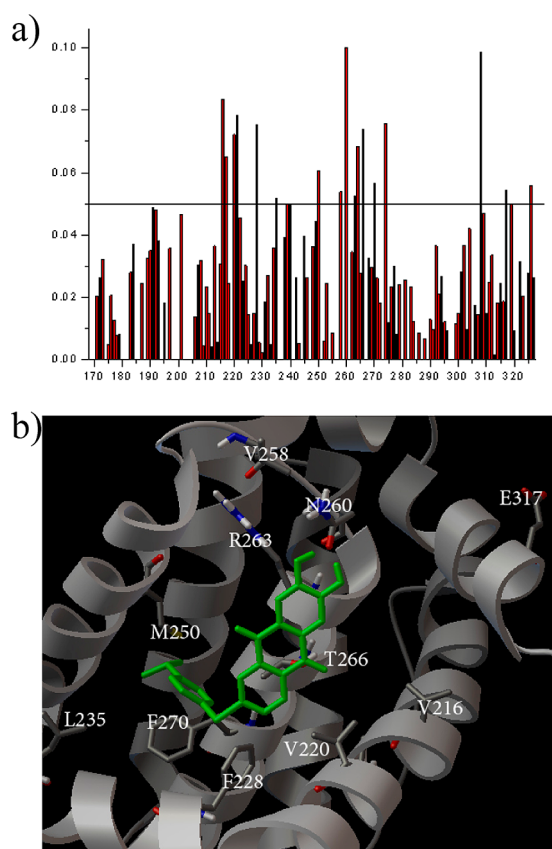


Figure 3. (a) Chemical shift perturbations of Mcl-1 residues bound to compound **6**. (b) NMR-derived structure of **6** bound to Mcl-1. Residues with $\Delta\text{CS} > 0.05$ ppm are shown. M250 and F270, representing the p2 pocket, are newly involved in binding.

CONCLUSIONS

In summary, we have constructed a novel rigid-plan small molecule scaffold **5** to mimic the structural and recognized binding features on two faces of the Bim BH3 α -helix. This scaffold is able to maintain its two-face binding mode and serves as a platform for further molecular evolution, leading to novel Bcl-2/Mcl-1 dual inhibitors with optimized affinities and pharmaceutical properties. Compound **6**, for example, was derived from **5** as a putative Bim mimetic and dual inhibitor with improved nanomolar affinity. The results reported here expand the range of small-molecule BH3 mimetics previously considered able to mimic only one face of the α -helix.

EXPERIMENTAL SECTION

Purity of all final products was determined by analytical HPLC to be $\geq 95\%$. HPLC purity of compounds was measured with a normal-phase HPLC (XBridge C18, 4.6×150 mm, $5 \mu\text{m}$) with two diverse wavelength detection systems. Compounds were eluted by gradient elution of 40/60 to 0/100 $\text{H}_2\text{O}/\text{CH}_3\text{OH}$ over 30 min at a flow rate of 0.3 mL/min.

General Procedure for Preparation of Compounds 1–4. A mixture of anhydrous AlCl_3 (18 g) and prebaked NaCl (4 g) was heated (110°C) in an oil bath until molten. A homogeneous mixture of phthalic anhydrides (888 mg, 6 mmol) and substituted phenols (6 mmol) separately were reacted with the $\text{AlCl}_3/\text{NaCl}$ melt. The temperature was slowly increased and maintained at 165°C for 4 h. The reaction mixture was cooled to 20°C , 10 mL of 10% HCl was added, and the mixture was stirred for 15 min at 20°C and then refluxed at 100°C for 30 min. The reaction mixture was cooled to room temperature and extracted with ethyl acetate. The resulting

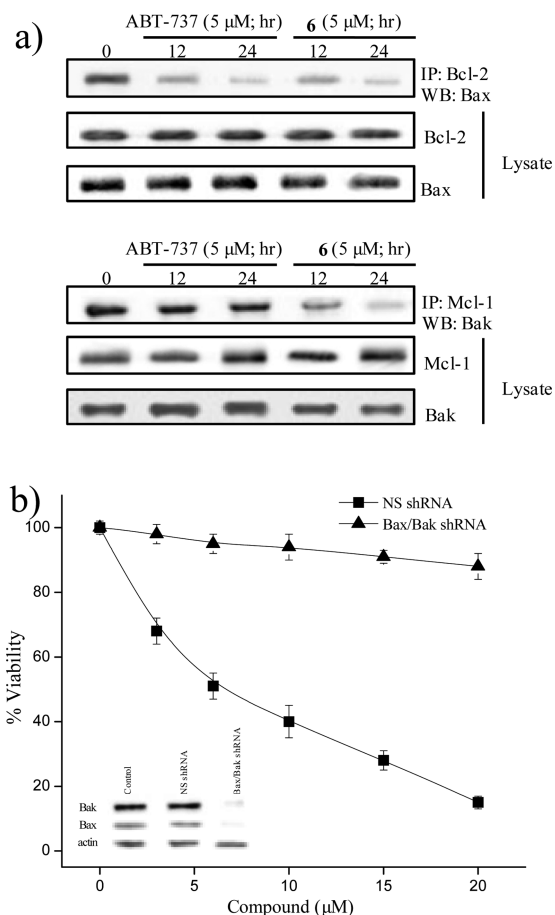


Figure 4. (a) Compound **6** interferes with Bcl-2/Bax and Mcl-1/Bak interactions in Nalm-6 cells. Nalm-6 cells were incubated with $5 \mu\text{M}$ ABT-737 and **6**, respectively, for 12 or 24 h, after which time total cell lysates were subjected to coimmunoprecipitation with anti-Bcl-2 or anti-Mcl-1 antibody. The precipitate and cell lysates were separated by sodium dodecyl sulfate–polyacrylamide gel electrophoresis (SDS–PAGE) and analyzed by Western blot with anti-Bcl-2, anti-Bax, anti-Mcl-1, and anti-Bak antibody. (b) MCF-7 cells transfected with NS shRNA or Bax/Bak shRNA were treated for 48 h with a graded dose of compound **6**, after which cell viability was determined by MTT assay.

product was purified by column chromatography on silica gel with chloroform and ethyl acetate as the mobile phase.

1,2,3-Trihydroxyanthracene-9,10-dione (1). Yield 690 mg, 45%; mp $282\text{--}284^\circ\text{C}$. ^1H NMR (400 MHz, in dimethyl sulfoxide, DMSO) δ 12.70 (s, 1H), 10.85 (s, 1H), 9.95 (s, 1H), 8.20 (t, $J = 8.0$ Hz, 1H), 8.14 (t, $J = 8.0$ Hz, 1H), 7.89 (d, $J = 12.0$ Hz, 2H), 7.27 (s, 1H). ^{13}C NMR (DMSO) 186.944, 180.962, 151.948, 151.766, 138.931, 134.556, 134.124, 133.214, 133.047, 126.618, 126.254, 124.655, 110.333, 108.809. Time-of-flight mass spectrometry with electron ionization [TOF MS (EI^+)] $\text{C}_{14}\text{H}_8\text{O}_5$, found 256.04. HPLC (40/60 to 0/100 $\text{H}_2\text{O}/\text{CH}_3\text{OH}$) purity = 98.56%, $t_{\text{R}} = 12.39$ min.

1,3-Dihydroxyanthracene-9,10-dione (2). Yield 375 mg, 28%; mp $218\text{--}219^\circ\text{C}$. ^1H NMR (400 MHz, DMSO) δ 12.74 (s, 1H), 11.34 (s, 1H), 8.19 (t, $J = 8.0$ Hz, 1H), 8.14 (t, $J = 8.0$ Hz, 1H), 7.91 (d, $J = 12.0$ Hz, 2H), 7.14 (s, 1H), 6.61 (s, 1H). ^{13}C NMR (DMSO) 185.886, 180.952, 165.457, 164.756, 134.935, 134.675, 134.473, 132.987, 132.870, 126.821, 126.349, 109.358, 108.392. TOF MS (EI^+) $\text{C}_{14}\text{H}_8\text{O}_4$, found 240.06. HPLC (40/60 to 0/100 $\text{H}_2\text{O}/\text{CH}_3\text{OH}$) purity = 97.32%, $t_{\text{R}} = 14.63$ min.

2,3-Dihydroxyanthracene-9,10-dione (3). Yield 216 mg, 15%; mp $259\text{--}262^\circ\text{C}$. ^1H NMR (400 MHz, DMSO) δ 10.63 (s, 2H), 8.13 (t, $J = 8.0$ Hz, 2H), 7.86 (t, $J = 8.0$ Hz, 2H), 7.53 (s, 2H). ^{13}C NMR (DMSO) 181.660, 151.592, 134.003, 133.222, 134.003, 133.222,

126.884, 126.429, 112.941. TOF MS (EI^+) $\text{C}_{14}\text{H}_8\text{O}_4$, found 240.03. HPLC (40/60 to 0/100 $\text{H}_2\text{O}/\text{CH}_3\text{OH}$) purity = 96.98%, t_{R} = 13.42 min.

1,2-Dihydroxyanthracene-9,10-dione (4). Yield 518 mg, 36%; mp 186–189 °C. ^1H NMR (400 MHz, DMSO) δ 12.61 (s, 1H), 10.89 (s, 1H), 8.25 (m, J = 8.0 Hz, 1H), 8.19 (m, J = 8.0 Hz, 1H), 7.93 (m, J = 12.0 Hz, 2H), 7.69 (d, J = 8.0 Hz, 1H), 7.24 (d, J = 8.0 Hz, 1H). ^{13}C NMR (DMSO) 189.30, 181.10, 153.25, 151.24, 135.63, 134.58, 134.07, 133.37, 127.23, 127.00, 124.30, 121.65, 121.33, 116.78. TOF MS (EI^+) $\text{C}_{14}\text{H}_8\text{O}_4$, found 240.08. HPLC (40/60 to 0/100 $\text{H}_2\text{O}/\text{CH}_3\text{OH}$) purity = 97.69%, t_{R} = 15.87 min.

General Procedure for Preparation of Compounds 5–9. To sodium hydroxide (2.4 g, 0.06 mol) dissolved in water (20 mL) was added phthalic anhydride (4.44 g, 0.03 mol). When complete solution was obtained, bromine (9.4 g, 3 mL, 0.06 mol) was incrementally added, while stirring, over 1 h. The reaction mixture was heated to 90 °C and allowed to react under reflux for 6 h. After 10 h of standing, the white solids that crystallized out of solution were filtered, washed with cold water, and analyzed as 4-bromophthalic acid salt. The total product was dissolved in hot water, and the pH was adjusted to about 1.5 by addition of concentrated HCl. The resulting solution was evaporated to dryness on a rotary evaporator and extracted with acetone to give 4-bromophthalic acid. Yield 5.0 g, 68%; mp 164–166 °C.

A solution of 4-bromophthalic acid (5 g, 0.02 mol) and acetic anhydride (30 mL) was heated for 2 h at 140 °C. The reaction mixture was cooled to room temperature and the excess acetic anhydride was removed under reduced pressure. The residue was washed with petroleum ether, and 4-bromophthalic anhydride was obtained as a white solid. Yield 3.8 g, 84%; mp 104–106 °C.

A mixture of anhydrous AlCl_3 (18 g) and prebaked NaCl (4 g) was heated (110 °C) in an oil bath until molten. A homogeneous mixture of 5-bromoisobenzofuran-1,3-dione (1.36 g, 6 mmol) and pyrocathechol (660 mg, 6 mmol) separately were reacted with the $\text{AlCl}_3/\text{NaCl}$ melt. The temperature was slowly increased and maintained at 165 °C for 4 h. The reaction mixture was cooled to 20 °C, 10 mL of 10% HCl was added, and the mixture was stirred for 15 min at room temperature and refluxed at 100 °C for 30 min. The reaction mixture was cooled to room temperature and extracted with ethyl acetate. The resulting product was purified by column chromatography on silica gel with ethyl acetate/petroleum ether (1:1) as the mobile phase.

A mixture of 6-bromo-2,3-dihydroxyanthracene-9,10-dione (160 mg, 0.5 mmol), corresponding benzenethiol (3 mmol), CuI (10 mg), and K_2CO_3 (69 mg, 0.5 mmol) was stirred in *N,N*-dimethylformamide (DMF) (20 mL) for 8 h at 140 °C. After being cooled to room temperature, the solution was poured into 10% HCl (20 mL), followed by extraction with ethyl acetate (3 \times 20 mL). The organic layer was collected and dried with MgSO_4 . After evaporation under reduced pressure, the product was purified by column chromatography on silica gel with ethyl acetate/petroleum ether (1:1).

6-Bromo-2,3-dihydroxyanthracene-9,10-dione (5). Yield 248 mg, 13%; mp 238–242 °C. ^1H NMR (400 MHz, DMSO) δ 10.60 (d, J = 12.0 Hz, 2H), 8.18 (d, J = 8.0 Hz, 1H), 8.04 (d, J = 8.0 Hz, 2H), 7.51 (s, 2H). ^{13}C NMR (DMSO) 181.40, 180.93, 152.40, 152.24, 137.08, 135.14, 132.61, 129.26, 129.21, 128.49, 127.24, 127.04, 113.46. TOF MS (EI^+) $\text{C}_{14}\text{H}_7\text{BrO}_4$, found 318.10, 320.04. HPLC (40/60 to 0/100 $\text{H}_2\text{O}/\text{CH}_3\text{OH}$) purity = 98.79%, t_{R} = 13.96 min.

2,3-Dihydroxy-6-(4-isopropylphenylthio)anthracene-9,10-dione (6). Yield 90 mg, 46%; mp 265–267 °C. ^1H NMR (400 MHz, DMSO) δ 10.62 (d, J = 12.0 Hz, 2H), 8.01 (d, J = 8.0 Hz, 1H), 7.68 (s, 1H), 7.53 (m, J = 8.0 Hz, 4H), 7.49 (s, 1H), 7.43 (m, J = 8.0 Hz, 2H), 2.97 (m, J = 16.0 Hz, 1H), 1.25 (d, J = 8.0 Hz, 6H). ^{13}C NMR (DMSO) 180.121, 180.841, 151.736, 151.432, 150.325, 150.325, 146.050, 134.526, 133.593, 130.871, 130.348, 128.309, 127.399, 126.906, 126.656, 126.542, 112.919, 33.192, 23.640. TOF MS (EI^+) $\text{C}_{23}\text{H}_{18}\text{O}_4\text{S}$, found 390.12. HPLC (40/60 to 0/100 $\text{H}_2\text{O}/\text{CH}_3\text{OH}$) purity = 98.15%, t_{R} = 14.58 min.

2,3-Dihydroxy-6-(phenylthio)anthracene-9,10-dione (7). Yield 43 mg, 24.7%; mp 251–253 °C. ^1H NMR (400 MHz, DMSO) δ 10.61 (d, J = 12.0 Hz, 2H), 8.02 (d, J = 8.0 Hz, 1H), 7.68 (s, 1H), 7.60 (m, J

= 12.0 Hz, 3H) 7.56 (m, J = 12.0 Hz, 3H), 7.49 (s, 1H), 7.46 (s, 1H). ^{13}C NMR (DMSO) 181.60, 181.36, 152.21, 151.93, 146.34, 145.97, 134.71, 134.14, 131.88, 131.03, 130.76, 130.58, 130.19, 127.97, 127.40, 127.04, 123.95, 113.41, 113.39. TOF MS (EI^+) $\text{C}_{20}\text{H}_{12}\text{O}_4\text{S}$, found 348.07. HPLC (40/60 to 0/100 $\text{H}_2\text{O}/\text{CH}_3\text{OH}$) purity = 97.62%, t_{R} = 14.07 min.

2,3-Dihydroxy-6-(*p*-tolylthio)anthracene-9,10-dione (8). Yield 67 mg, 37%; mp 256–258 °C. ^1H NMR (400 MHz, DMSO) δ 10.63 (d, J = 12.0 Hz, 2H), 8.00 (d, J = 8.0 Hz, 1H), 7.63 (s, 1H), 7.52 (m, J = 8.0 Hz, 4H), 7.45 (s, 1H), 7.37 (m, J = 8.0 Hz, 2H), 2.51 (s, 3H). ^{13}C NMR (DMSO) 181.174, 180.886, 151.743, 151.432, 146.383, 139.878, 134.746, 133.608, 130.993, 130.280, 127.414, 126.914, 126.542, 126.065, 126.065, 122.744, 112.903, 62.783. TOF MS (EI^+) $\text{C}_{21}\text{H}_{14}\text{O}_4\text{S}$, found 362.09. HPLC (40/60 to 0/100 $\text{H}_2\text{O}/\text{CH}_3\text{OH}$) purity = 98.16%, t_{R} = 14.45 min.

6-(4-Bromophenylthio)-2,3-dihydroxyanthracene-9,10-dione (9). Yield 51 mg, 23.9%; mp 258–262 °C. ^1H NMR (400 MHz, DMSO) δ 10.62 (d, J = 12.0 Hz, 2H), 8.03 (d, J = 8.0 Hz, 1H), 7.73 (d, J = 8.0 Hz, 2H), 7.49 (m, J = 8.0 Hz, 4H), 7.36 (m, J = 8.0 Hz, 2H). ^{13}C NMR (DMSO) 181.55, 181.32, 152.24, 151.97, 145.18, 144.87, 137.55, 136.26, 135.27, 134.19, 133.67, 133.29, 133.16, 132.46, 132.36, 131.40, 128.08, 127.04, 123.58, 113.42. TOF MS (EI^+) $\text{C}_{20}\text{H}_{11}\text{BrO}_4\text{S}$, found 426.97. HPLC (40/60 to 0/100 $\text{H}_2\text{O}/\text{CH}_3\text{OH}$) purity = 96.82%, t_{R} = 14.12 min.

■ ASSOCIATED CONTENT

📄 Supporting Information

Additional text, seven figures, and one table with experimental procedures and full spectroscopic data for all new compounds. This material is available free of charge via the Internet at <http://pubs.acs.org>.

■ AUTHOR INFORMATION

Corresponding Author

*E-mail zc Zhang@dlut.edu.cn; fax 86-411-84986032; tel 86-411-84986032.

Notes

The authors declare no competing financial interest.

■ ACKNOWLEDGMENTS

The work was supported by the National Natural Science Foundation of China (81273436 and 81272876).

■ REFERENCES

- (1) Ryan, D. P.; Matthews, J. M. Protein–protein interactions in human disease. *Curr. Opin. Struct. Biol.* **2005**, *15*, 441–446.
- (2) Shaginian, A.; Whitby, L. R.; Hong, S.; Hwang, I.; Farooqi, B.; Searcey, M.; Chen, J. D.; Vogt, P. K.; Boger, D. L. Design, synthesis, and evaluation of an alpha-helix mimetic library targeting protein–protein interactions. *J. Am. Chem. Soc.* **2009**, *131*, 5564–5572.
- (3) Bullock, N.; Jochim, A. J.; Arora, P. S. Assessing helical protein interfaces for inhibitor design. *J. Am. Chem. Soc.* **2011**, *133*, 14220–14223.
- (4) Jochim, L.; Arora, P. S. Systematic analysis of helical protein interfaces reveals targets for synthetic inhibitors. *ACS Chem. Biol.* **2010**, *5*, 919–923.
- (5) Lee, E. F.; Czabotar, P. E.; Van Delft, M. F.; Michalak, E. M.; Boyle, M. J.; Willis, S. N.; Puthalakath, H.; Bouillet, P.; Colman, P. M.; Huang, D. C. S.; Fairlie, W. D. A novel BH3 ligand that selectively targets Mcl-1 reveals that apoptosis can proceed without Mcl-1 degradation. *J. Cell Biol.* **2008**, *180*, 341–355.
- (6) Degterev, A.; Boyce, M.; Yuan, J. The channel of death. *J. Cell Biol.* **2001**, *155*, 695–698.
- (7) Wei, M. C.; Zong, W.-X.; Cheng, E. H.-Y.; Lindsten, T.; Panoutsakopoulou, V.; Ross, A. J.; Roth, K. A.; MacGregor, G. R.; Thompson, C. B.; Korsmeyer, S. J. Proapoptotic BAX and BAK: A

requisite gateway to mitochondrial dysfunction and death. *Science* **2001**, *292*, 727–730.

(8) Scorrano, L.; Oakes, S. A.; Opferman, J. T.; Cheng, E. H.; Sorcinelli, M. D.; Pozzan, T.; Korsmeyer, S. J.. BAX and BAK regulation of endoplasmic reticulum Ca^{2+} : a control point for apoptosis. *Science* **2003**, *300*, 135–139.

(9) Lee, E. F.; Czabotar, P. E.; Smith, B. J.; Deshayes, K.; Zobel, K.; Colman, P. M.; Fairlie, W. D. Crystal structure of ABT-737 complexed with Bcl-xL: implications for selectivity of antagonists of the Bcl-2 family. *Cell Death Differ.* **2007**, *14*, 1711–1713.

(10) Schafmeister, C. E.; Po, J.; Verdine, G. L. An all-hydrocarbon cross-linking system for enhancing the helicity and metabolic stability of peptides. *J. Am. Chem. Soc.* **2000**, *122*, 5891–5892.

(11) Boersma, M. D.; Haase, H. S.; Peterson-Kaufman, K. J.; Lee, E. F.; Clarke, O. B.; Colman, P. M.; Smith, B. J.; Horne, W. S.; Fairlie, W. D.; Gellman, S. H. Evaluation of diverse α/β -backbone patterns for functional α -helix mimicry: Analogues of the Bim BH3 domain. *J. Am. Chem. Soc.* **2012**, *134*, 315–323.

(12) Petros, M.; Dinges, J.; Suger, D. J.; Baumeister, S. A.; Betebenner, D. A.; Bures, M. G.; Elmore, S. W.; Hajduk, P. J.; Joseph, M. K.; Fesik, S. W. Discovery of a potent inhibitor of the antiapoptotic protein Bcl-xL from NMR and parallel synthesis. *J. Med. Chem.* **2006**, *49*, 656–663.

(13) Wei, J.; Rega, M. F.; Kitada, S.; Yuan, H.; Zhai, D.; Risbood, P.; Seltzman, H. H.; Twine, C. E.; Reed, J. C.; Pellecchia, M. Synthesis and evaluation of Apogossypol atropisomers as potential Bcl-xL antagonists. *Cancer Lett.* **2009**, *273*, 107–113.

(14) Kitada, S.; Leone, M.; Sareth, S.; Zhai, D.; Reed, J. C.; Pellecchia, M. Discovery, characterization, and structure–activity relationships studies of proapoptotic polyphenols targeting B-cell lymphocyte/leukemia-2 proteins. *J. Med. Chem.* **2003**, *46*, 4259–4264.

(15) Becattini, B.; Kitada, S.; Leone, M.; Monosov, E.; Chandler, S.; Zhai, D.; Kipps, T. J.; Reed, J. C.; Pellecchia, M. Rational design and real time, in-cell detection of the proapoptotic activity of a novel compound targeting Bcl-X(L). *Chem. Biol.* **2004**, *11*, 389–395.

(16) Tosovska, P.; Arora, P. S. Oligoaxopiperazines as nonpeptidic α -helix mimetics. *Org. Lett.* **2010**, *12*, 1588–1591.

(17) Restorp, P.; Rebek, J. J. Synthesis of α -helix mimetics with four side-chains. *Bioorg. Med. Chem. Lett.* **2008**, *18*, 5909–5911.

(18) Bruncko, M.; Oost, T. K.; Belli, B. A.; Ding, H.; Joseph, M. K.; Kunzer, A.; Martineau, D.; McClellan, W. J.; Mitten, M.; Ng, S. C.; Nimmer, P. M.; Oltersdorf, T.; Park, C. M.; Petros, A. M.; Shoemaker, A. R.; Song, X.; Wang, X.; Wendt, M. D.; Zhang, H.; Fesik, S. W.; Rosenberg, S. H.; Elmore, S. W. Studies leading to potent, dual inhibitors of Bcl-2 and Bcl-XL. *J. Med. Chem.* **2007**, *50*, 641–646.

(19) Petros, M.; Olejniczak, E. T.; Fesik, S. W. Structural biology of the Bcl-2 family of proteins. *Biochim. Biophys. Acta* **2004**, *1644*, 83–94.

(20) Liu, Q.; Moldoveanu, T.; Sprules, T.; Matta-Camacho, E.; Mansur-Azzam, N.; Gehring, K. Apoptotic regulation by MCL-1 through heterodimerization. *J. Biol. Chem.* **2010**, *285*, 19615–19624.

(21) Zhang, C.; Wu, G. Y.; Xie, F. B.; Ting, S.; Chang, X. L. 3-Thiomorpholin-8-oxo-8H-acenaphtho[1,2-*b*]pyrrole-9-carbonitrile (S1) based molecules as potent, dual inhibitors of B-cell lymphoma 2 (Bcl-2) and myeloid cell leukemia sequence 1 (Mcl-1): structure-based design and structure–activity relationship studies. *J. Med. Chem.* **2011**, *54*, 1101–1105.

(22) Freire, E. Do enthalpy and entropy distinguish first in class from best in class. *Drug Discovery Today* **2008**, *13*, 869–874.

(23) Ferenczy, G. G.; Keseru, G. M. Thermodynamics guided lead discovery and optimization. *Drug Discovery Today* **2010**, *15*, 919–932.

(24) Hang, Y.; Lee, G. I.; Sedey, K. A.; Rodriguez, J. M.; Wang, H. G.; Sebt, S. M.; Hamilton, A. D. Terephthalamide derivatives as mimetics of helical peptides: disruption of the Bcl-x(L)/Bak interaction. *J. Am. Chem. Soc.* **2005**, *127*, 5463–5468.

(25) Maringanti, S.; Cheemala, M. N.; Ahn, J. M. Novel amphiphilic α -helix mimetics based on a bis-benzamide scaffold. *Org. Lett.* **2009**, *11*, 4418–4421.

(26) Tang, G. Z.; Ding, K.; Zaneta, N. C.; Yang, C. Y.; Qiu, S.; Shangary, S.; Wang, R. X.; Guo, J.; Gao, W.; Wang, G. P.; Meagher, J.;

Stuckey, J.; Krajewski, K.; Jiang, S.; Roller, P. P.; Wang, S. M. Structure-based design of flavonoid compounds as a new class of small-molecule inhibitors of the anti-apoptotic Bcl-2 proteins. *J. Med. Chem.* **2007**, *50*, 3163–3166.

(27) Dhananjeyan, M. R.; Milev, Y. P.; Kron, M. A.; Nair, M. G. Synthesis and activity of substituted anthraquinones against a human filarial parasite, *Brugia malayi*. *J. Med. Chem.* **2005**, *48*, 2822–2830.

(28) Oltersdorf, T.; Elmore, S. W.; Shoemaker, A. R.; Shoemaker, A. R.; Armstrong, R. C.; Augeri, D. J.; Belli, B. A.; Bruncko, M.; Deckwerth, T. L.; Dinges, J.; Hajduk, P. J.; Joseph, M. K.; Kitada, S.; Korsmeyer, S. J.; Kunzer, A. R.; Letai, A.; Li, C.; Mitten, M. J.; Nettesheim, D. G.; Ng, S. C.; Nimmer, P. M.; Connor, J. M.O.; Oleksijew, A.; Petros, A. M.; Reed, J. C.; Shen, W.; Tahir, S. K.; Thompson, C. B.; Tomaselli, K. J.; Wang, B.; Wendt, M. D.; Zhang, H.; Fesik, S. W.; Rosenberg, S. H. An inhibitor of Bcl-2 family proteins induces regression of solid tumors. *Nature* **2005**, *435*, 677–681.